Fluorinated Alcohol Biosolvents and α-Helix Peptide Secondary Structure: A Molecular Dynamics Study on the Solvent Concentration

liquids

MDPI

Article

Fluorinated Alcohol Biosolvents and α-Helix Peptide Secondary Structure: A Molecular Dynamics Study on the Solvent Concentration Effect

Michele Casoria [1], Marco Pagliai [1], Claudia Andreini [1,2], Anna Maria Papini [1,3], Piero Procacci [1] and Marina Macchiagodena [1,*]

[1] Dipartimento di Chimica "Ugo Schiff", Università degli Studi di Firenze, Via della Lastruccia 3, 50019 Sesto Fiorentino, Italy; michele.casoria@unifi.it (M.C.); marco.pagliai@unifi.it (M.P.); claudia.andreini@unifi.it (C.A.); annamaria.papini@unifi.it (A.M.P.); piero.procacci@unifi.it (P.P.)
[2] Magnetic Resonance Center (CERM), Università degli Studi di Firenze, Via Luigi Sacconi 6, 50019 Sesto Fiorentino, Italy
[3] Interdepartmental Research Unit of Peptide and Protein Chemistry and Biology, Università degli Studi di Firenze, Via della Lastruccia 13, 50019 Sesto Fiorentino, Italy
* Correspondence: marina.macchiagodena@unifi.it

Abstract

An upgraded GAFF2 force field has been used to simulate two fluorinated alcohols, TFE and HFIP, in aqueous solutions at several concentrations. The same force field has also been employed to simulate a 26-residue amphiphilic peptide in several cosolvent/water mixtures to verify and clarify its efficacy in stabilizing the secondary structure. The calculated thermodynamic and structural properties are in agreement with experimental findings. The force field allows a correct description of the secondary structure and affords an accurate characterization of the spatial organization of cosolvent molecules around the peptide.

Keywords: biosolvents; force field; molecular dynamics simulations; TFE; HFIP; secondary structure; peptide; GAFF2

1. Introduction

2,2,2-Trifluoroethanol (TFE) and 1,1,1,3,3,3-Hexafluoro-2-propanol (HFIP) are two fluorinated alcohols used as cosolvents for structural stabilization of secondary structure-forming peptides. In particular, NMR and CD studies show that their presence increases the population of α-helix and β-sheet content [1–3]. The factors influencing the efficacy of structure-inducing cosolvents are their concentration in aqueous solution and the amino acid sequence of the peptide. Computational and experimental techniques have investigated the mechanism of peptide stabilization by fluorinated solvents [2–5]. As stated in the review [2], there is as yet no single mechanism that accounts for all of the effects TFE and related cosolvents have on polypeptide conformation. In an early MD study of Mellitin in 30% (vol/vol) TFE/water mixtures, Roccatano et al. proposed a helix stabilization mechanism whereby a layer of cosolvent molecules is formed around the peptide, which reduces the accessibility of water molecules and, consequently, increases the stability of the intermolecular hydrogen bonds between carbonyl and amide NH groups, as well as the secondary structure. In addition, the cosolvent molecules' layer causes a lowering of the dielectric constant. The formation of clusters of cosolvent molecules has also been described in water as the concentration of the organic cosolvent increases [3].

Academic Editor: Darin J. Ulness

Received: 10 October 2025
Revised: 31 December 2025
Accepted: 19 January 2026
Published: 23 January 2026

To study the structural and dynamic properties of peptides in biomimetic media and cosolvent molecules in water at the molecular level, molecular dynamics (MD) simulations can be used [4,6,7]. To accurately reproduce experimental findings, MD simulations need an accurate force field (FF) [8–11], which is characterized by a set of functional forms with a minimal set of adjustable parameters. In the present study, we make use of the refined FF recently proposed by some of us for TFE, HFIP, and 1,1,1,3,3,3-hexafluoropropan-2-one (HFA) fluorinated alcohols [12]. The upgraded FF is based on General AMBER Force Field 2 [13] with parameterization of atomic charges using ab initio calculations on stable conformers previously identified using single-point energy evaluations on selected dihedral angles. To verify the accuracy of the FF in describing the structural and thermodynamic properties of cosolvent/water solutions, MD simulations with the upgraded FF were performed on TFE and HFIP water solutions with a concentration from 0 to 100% of TFE and HFIP. Furthermore, to study the secondary structure stabilization effect, MD simulations were performed on cosolvent/water solutions with a peptide. The peptide used was Mellitin (MLT), which is a 26-residue amphiphilic peptide (GIGAVLKVLTTGLPALISWIKRKRQQ) and is the principal component of the venom of *Apis mellifera*. In pure water, at pH 4, MLT is unfolded [14], while it assumes a helical conformation when it is bound to the membrane as well as in alcohol solutions. [15] MLT consists of two α-helical regions, and these portions are connected by the residues Thr-11 and Gly-12.

This paper is organized as follows. In Section 2, we describe MD simulations in some detail. In Section 3, we present the results obtained using the upgraded FF and a critical assessment of them. Conclusive remarks and perspectives are discussed in Section 4.

2. Methods

Molecular Dynamics Simulations

To study the properties of cosolvent/water solutions, we used concentrations of 10%, 20%, 30%, 40%, 50%, 60%, 70%, 80%, and 90% (v/v) of TFE and HFIP. In addition, we also considered a pure solution of TFE and HFIP (molecular structure in Figure 1).

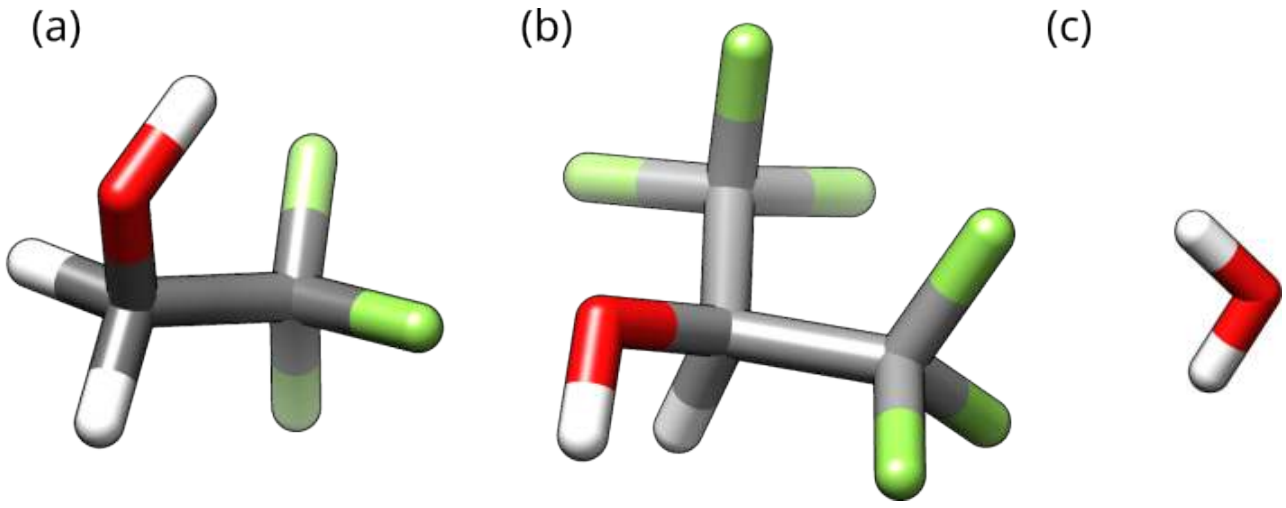

Figure 1. Molecular structure of TFA (**a**), HFIP (**b**), and water (**c**).

To obtain the different concentrations of cosolvent/water solutions, we used the number of cosolvent and water molecules reported in Table 1. The total number of molecules for all the simulated systems was 6000. The starting coordinates were generated using GROMACS standard tools [16] and inserting a specified number of molecules in random positions.

Table 1. Summary of the composition of simulated systems; N. water and N. cosolvent indicate the number of water and cosolvent molecules, respectively.

% (*v*/*v*)	TFE Mixture		HFIP Mixture	
	N. Water	N. Cosolvent	N. Water	N. Cosolvent
10	5838	162	5886	114
20	5646	354	5754	246
30	5418	582	5592	408
40	5142	858	5382	618
50	4800	1200	5124	876
60	4362	1638	4770	1230
70	3786	2214	4284	1716
80	3000	3000	3558	2442
90	1842	4158	2358	3642
100	0	6000	0	6000

For the simulation of MLT in cosolvent/water mixtures, we considered 10:90, 20:80, 30:70, 40:60, and 50:50 (*v*/*v*) cosolvent/water solutions, maintaining the same number of TFE, HFIP, and H_2O molecules reported in Table 1. MLT (pdb identification code 2MLT) was parametrized using AMBER99SB-ILDN FF [17]; the two cosolvents with the upgraded FF [12]; and the water molecules with the 3-site TIP3P model [18,19]. For all systems, simulations were performed with a cubic box with periodic boundary conditions using GROMACS 2025.1 [16]. First, the steepest descent energy minimization was applied. The systems were then heated to 298.15 K for 1 ns while keeping the temperature constant using a V-rescale [20] with a coupling time constant of 1 ps. The resulting configuration was used as a starting point for an NPT simulation (using the C-rescale exponential relaxation pressure coupling) with a period of pressure fluctuations at the equilibrium setting of 2.0 ps until the systems were allowed to converge to uniform density (2 ns, time-step 1 fs). The production run in the NPT ensemble was carried out for 100 ns with δt = 2.0 fs, imposing rigid constraints only on the X–H bonds (with X being any heavy atom) by means of the LINCS algorithm [21]. In addition to the calculation of the static dielectric constant, we also performed an NVT ensemble simulation (2 ns, time-step 1 fs) starting from the last configuration of the previous NPT simulation. For all simulations, electrostatic interactions were evaluated using the particle-mesh Ewald (PME) [22] method with a grid spacing of 1.2 Å, a real-space cutoff of 1.2 nm, and a spline interpolation of order 4. Van der Waals interactions were calculated using a cut-off of 1.0 nm. Long-range dispersion corrections for Lennard-Jones interactions were used for energy and pressure [16,23]. The procedure just described was performed considering the two cosolvents and several cosolvent/water solutions; therefore, we conducted an extensive study using 3.1 µs atomic-detail molecular dynamics simulations.

Static dielectric constant (ϵ), excess enthalpy (ΔH_{mix}), density (ρ), Root Mean Square Deviation (RMSD), and intermolecular radial distribution functions (RDFs) were determined using GROMACS standard tools [16]. In particular for ϵ calculation, the total dipole plus fluctuations was used for the estimation according to Equation (1):

$$\epsilon = 1 + \frac{4\pi}{3 < V > k_B T}(< M^2 > - < M >^2); M = \sum_i \mu_i \quad (1)$$

where μ_i is the molecular dipole moment.

The secondary structure of MLT and its evolution were analyzed using the Define Secondary Structure of Proteins (DSSP) algorithm [24]. To describe the interaction of the peptide with the cosolvent, the Local Cosolvent Concentration (LCC) was evaluated from

the number of solvent and cosolvent molecules present in a shell of 6 Å around the peptide residues according to Equation (2) [25].

$$LCC(r) = \frac{V_m^c n_c(r)}{V_m^c n_c(r) + V_m^{H_2O} n_{H_2O}(r)} \quad (2)$$

where V_m^c and $V_m^{H_2O}$ represent the average excluded volumes of the cosolvent and water molecules, respectively. The corresponding values are 0.10 for HFIP, 0.07 for TFE, and 0.019 (L/mol) for water.

3. Results

3.1. Cosolvent/Water Solutions

In Figure 2 and in Table S1 of the Supporting Information (SI), we report the calculated thermodynamic properties for the cosolvent/water solutions.

For both cosolvents, the density increases and the static dielectric constant decreases with the concentration. The values of density and ϵ at 10% (v/v) concentration of TFE and HFIP highlight the distinct chemical and structural properties of the two cosolvents: TFE has a higher dipole moment and HFIP a higher molecular mass. The values at 50% and 100% (v/v) are in agreement with those reported in our previous paper [12]. The experimental values of density at 50% (v/v) are 1170 kg/m^3 and 1250 kg/m^3 [3,26–29] for TFE and HFIP, respectively, in agreement with the computed ones. An excellent agreement is found also for density values for TFE and HFIP pure solutions, for which experimental values are 1383 kg/m^3 and 1607 kg/m^3, respectively.

The excess enthalpy has a different trend for the two cosolvents, as shown in Figure 2c. For TFE, the calculated value increases up to a concentration of 80% (v/v) before decreasing. In contrast, for HFIP, the calculated ΔH_{mix} decreases with increasing concentration. The ΔH_{mix} is positive for TFE, whereas, for HFIP, we observe small positive values at lower concentrations and negative values at higher concentrations. This indicates that water and HFIP mix exothermically except at highly water-rich concentrations and water and TFE mix endothermically across all concentrations. The agreement between our findings and experimental data [30] is reasonable only for cosolvent-rich concentrations, but the computed ΔH_{mix} allows us to appreciate the type of chemical process when water and cosolvents are mixed at different concentrations in agreement with experiments.

The agreement between the computed and experimental static dielectric constant is worse than that of densities. Analyzing all the computed values reported in Figure 2a and in Table S1 of the SI, ϵ is overestimated for both cosolvents and for lower concentrations (10% and 20% (v/v)) and is underestimated for concentrations higher than 50%. The best agreement is obtained at 30%, 40%, and 50% (v/v) concentrations and especially for TFE. However, the difference between computed and experimental ϵ values was also found in previous studies. It was ascribed to insufficient sampling and/or to the absence of an explicit polarization term in the FF [6,7]. To obtain comparable values of ϵ using MD simulation is not easy, as was also pointed out in a paper by Caleman et al. [31], in which the dielectric constant was defined as "the hardest nut to crack" [32]. Furthermore, we also have to take into account the water model employed, which can affect the results. However, several efforts are being made to improve the determination of thermodynamic properties as an FF reparametrization employing ϵ as a target property [33,34].

In Figure 3, we report the RDFs between the center Of mass (COM) of TFE-TFE, TFE–water, HFIP-HFIP, and HFIP–water. In all the analyses, there is a dependence on the concentration of the cosolvents. The average number of TFE molecules at 7.2 Å (first minimum of the RDF) from a reference TFE molecule ranges from 1.6 to 12.3 for 10% (v/v)

to 100% (v/v) TFE/water solutions. A similar trend was also found for HFIP mixtures with an average number of HFIP at 8.4 Å, ranging from 3.5 to 13.2 for 10% (v/v) to 100% (v/v) HFIP/water solutions. As expected, an opposite trend was found for the average number of water molecules at 5.6 Å from a reference TFE molecule and at 6.7 Å from a reference HFIP molecule, with values ranging from 18.2 to 2.4 for TFE and from 25.8 to 4.2 for HFIP for 10% (v/v) to 90% (v/v) cosolvent/water solutions (all values are reported in Table S2 of the SI). To appreciate the corresponding organization of molecules in the solutions, Figures S1 and S2 of the SI show the final snapshot of MD simulations for three concentrations of cosolvent/water (10%, 50%, and 90% v/v) solutions. The formation of cosolvent clusters increases with the number of molecules and, for HFIP, is also observed at a lower concentration, confirming the different average number of molecules found at the first RDF minimum for the two cosolvents in 10% (v/v) solutions.

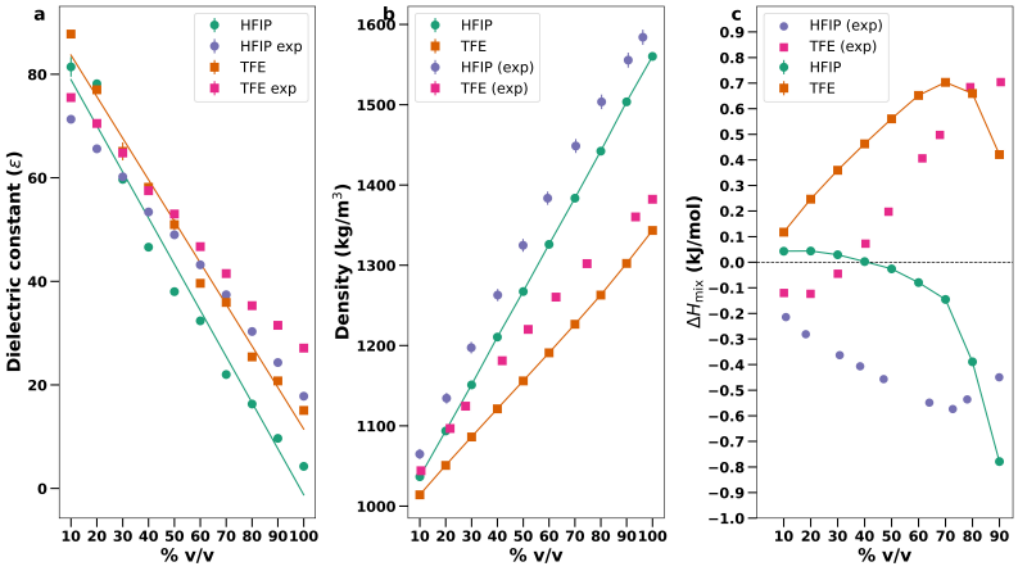

Figure 2. Calculated and experimental thermodynamic properties of cosolvent/water solutions of TFE and HFIP. In panel (**a**), the calculated and experimental dielectric constants are displayed. Panel (**b**) shows the computed densities (kg/m^3), while panel (**c**) displays the calculated and experimental excess enthalpies (kJ/mol). The experimental dielectric constant values are derived from Ref. [3]; experimental density is extracted from Refs. [35,36]; and experimental ΔH_{mix} is extracted from Ref. [30]. Calculated properties for TFE and HFIP are depicted by the orange squares and green dots, respectively, and the experimental data for TFE and HFIP are shown by the magenta squares and blue dots, respectively. Solid lines are a guide to the eye for computed data.

In Figure 4, we present the RDFs between the hydrogen atom of the hydroxyl group of the cosolvents and the oxygen atom of the water (refer to Figure 1 for the molecular structure). Additionally, we show the intermolecular g(r) between H_{water} and O_{water}. The (g(r)) functions are selected in accordance with previous work by some of us [12], in which we observed that the (g(r)) functions involving fluorine atoms exhibit only broad and small peaks. In all the RDFs, there is a noticeable dependence on the concentration of the cosolvents. Notably, the g(r) $H_{hydroxyl}\cdots O_{water}$ calculated for HFIP/water solutions is higher than the corresponding RDF for TFE/water solutions, which is consistent with ΔH_{min} data, indicating an exothermic process when HFIP is added to water. The g(r) $H_{water}\cdots O_{water}$ is comparable for the two cosolvents, showing the same average number of oxygen atoms at the first minimum, 2.5 Å. The values are 0.9, 0.8, 0.8, 0.8, 0.7, 0.7, 0.6, 0.4, and 0.2 for cosolvent/water concentrations from 10% to 90% (v/v). The values decrease in line with the number of cosolvent molecules.

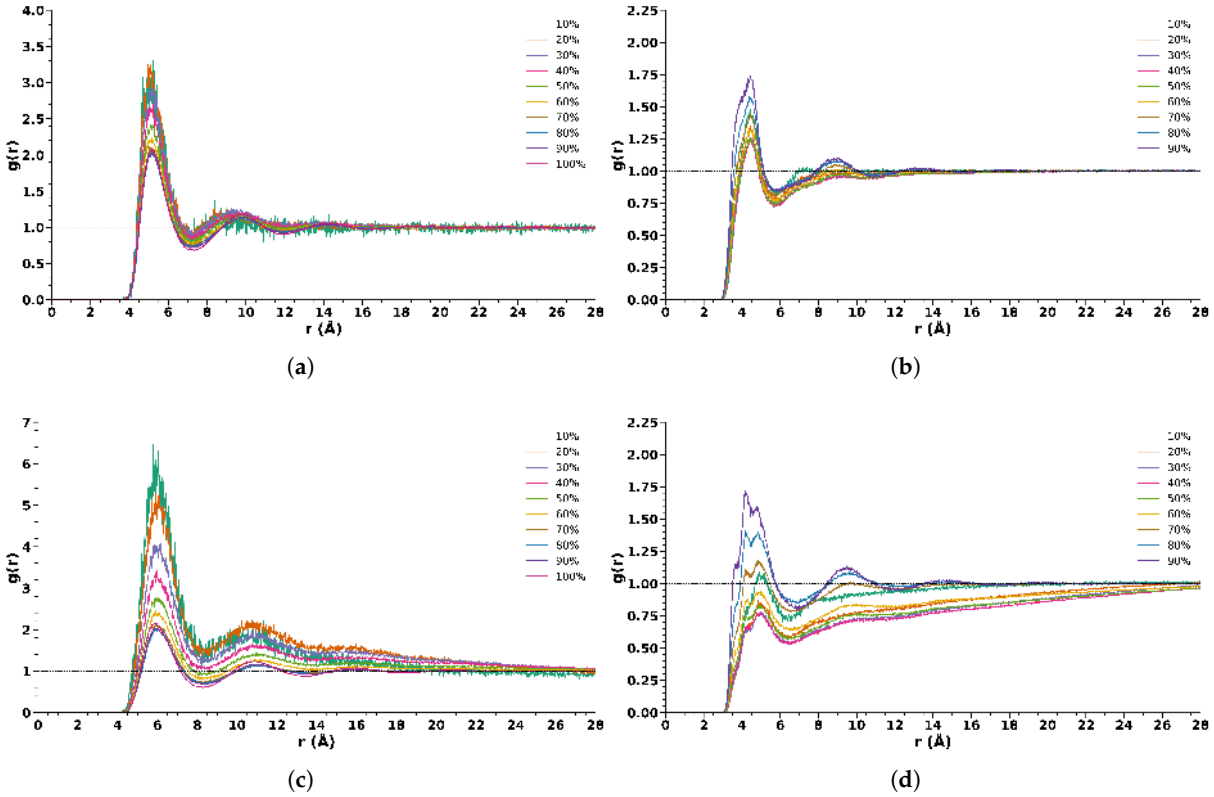

Figure 3. Radial distribution function between the center of mass of (**a**) TFE-TFE; (**b**) TFE–water; (**c**) HFIP-HFIP, and (**d**) HFIP–water for all the cosolvent/water concentrations.

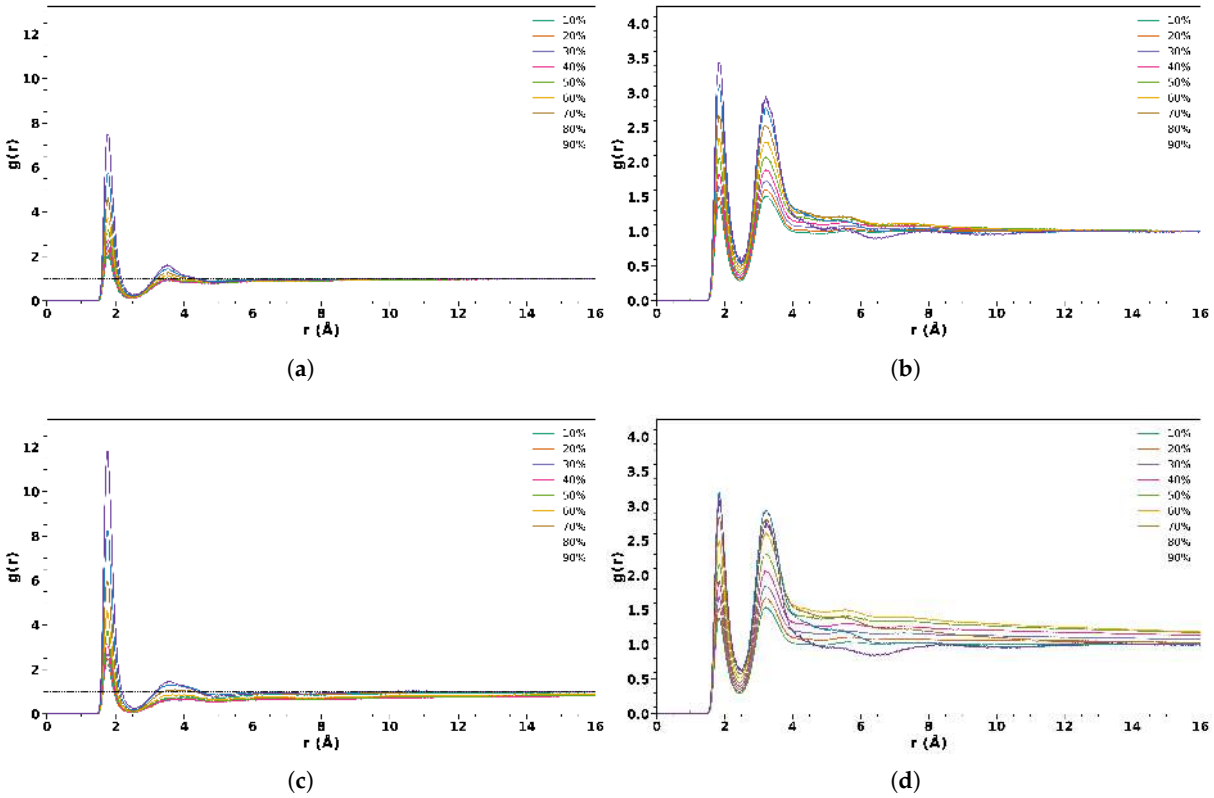

Figure 4. (**a**,**c**) are the radial distribution functions between the hydrogen atom of the hydroxyl group of the cosolvent and the oxygen atom of the water molecules. (**a**) refers to TFE and (**c**) to HFIP. (**b**,**d**) are the intermolecular radial distribution functions between the hydrogen and the oxygen atoms of water molecules. (**b**) refers to TFE solutions and (**d**) to HFIP solutions.

3.2. Melittin in Cosolvent/Water Solutions

To study the secondary structure stabilization effect of TFE and HFIP, we performed MD simulations of MLT peptide in five different cosolvent/water solutions (10%, 20%, 30%, 40%, and 50%) and in pure water, although some studies [3,37] suggest that a concentration of around 30% is optimal for inducing secondary structure stabilization in peptides and proteins. In Figure 5, we report the MLT backbone RMSD calculated at all concentrations for the two cosolvents. As expected, in water, the RMSD reaches the highest values during the 100 ns of the simulation. In TFE, the lower value is found when the MLT is dissolved in the 30% (v/v) cosolvent/water solution; in HFIP, the lower value is found when the concentration is 20%. Interestingly, for higher concentrations, such as 40% or 50% (v/v) cosolvent/water solutions, the RMSD is higher, although always lower than 0.7 Å. As Supplementary Materials, we provide an animated video showing how a region of the MLT unfolds in HFIP/water solutions at a concentration of 40% (v/v). To study in more detail the evolution of the MLT secondary structure, in Figure 6 we report the DSSP of MLT in water, 30% (v/v) TFE/water, and 30% (v/v) HFIP/water solutions (the results for the other concentrations are reported in Figures S3 to S10 of the SI). The DSSP calculation for MLT in aqueous solutions confirms the unstable structure already found in the RMSD analysis. The structure remains unstable throughout the simulation; a hint of an α-helix is observed in the region between Pro-14 and Trp-19, but it is not stable. For TFE and HFIP (30% (v/v)), a well-defined flexible region from Thr-11 to Leu-13 connects two α-helical regions. The two *alpha*-helices are stable during the 100 ns MD simulations. For the cosolvent concentrations lower than 30%, in HFIP we observe a similar pattern to the 30% (v/v) concentration, while in TFE the two α-helical regions involve a smaller number of amino acids, particularly in the first segment (from Gly-1 to Thr-10) where the first residues are disordered. In the concentration higher than 30%, in both cosolvents, the first segment exhibits disorder, and the flexible region connecting the two α-helical regions involves a larger number of aminoacids.

To verify the formation of a layer of cosolvent molecules around MLT, we calculated the LCC around the C_α atom of each residue of the peptide at 6 Å (Figure 7). For TFE, we found a marked change with the cosolvent concentration. For the 10% (v/v) concentration, the first and the last residues, as well as the connecting residues (Thr-11 and Gly-12), show lower values of LCC reaching the value of 50%. For the other concentrations, the values of LCC grow, retaining values of 50% and 60% for the first and last residues. The net decrease around the flexible region (Thr-11 and Ile-20) is evident for all the concentrations. For HFIP, we have a similar trend for all the concentrations: smaller values of LCC for the first two and the last three residues and a value around 90% for the residues from 5 to 21. Also in this case, we have a decrease around the flexible region (Thr-11 and Ile-20). The difference between the two solvents can be ascribed to the difference in the dipole moment and to the presence of two -CF_3 groups in HFIP. To illustrate the LCC results, Figure S11 in the Supplementary Information (SI) presents the final snapshot of the MLT MD simulations for two concentrations of cosolvent/water (10% and 50% v/v) solutions. The two cosolvents are arranged differently around MLT, with water molecules positioned closer to the first and last residues.

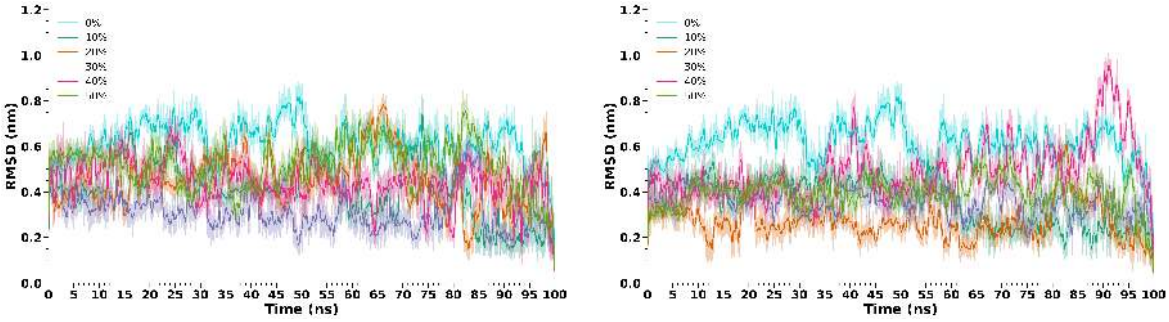

(**a**) (**b**)

Figure 5. RMSD values of the protein backbone for MLT in TFE solutions (**a**) and in HFIP solutions (**b**). In the plots, the results for pure water (0%) and for 10%, 20%, 30%, 40%, and 50% colvent/water concentrations are reported.

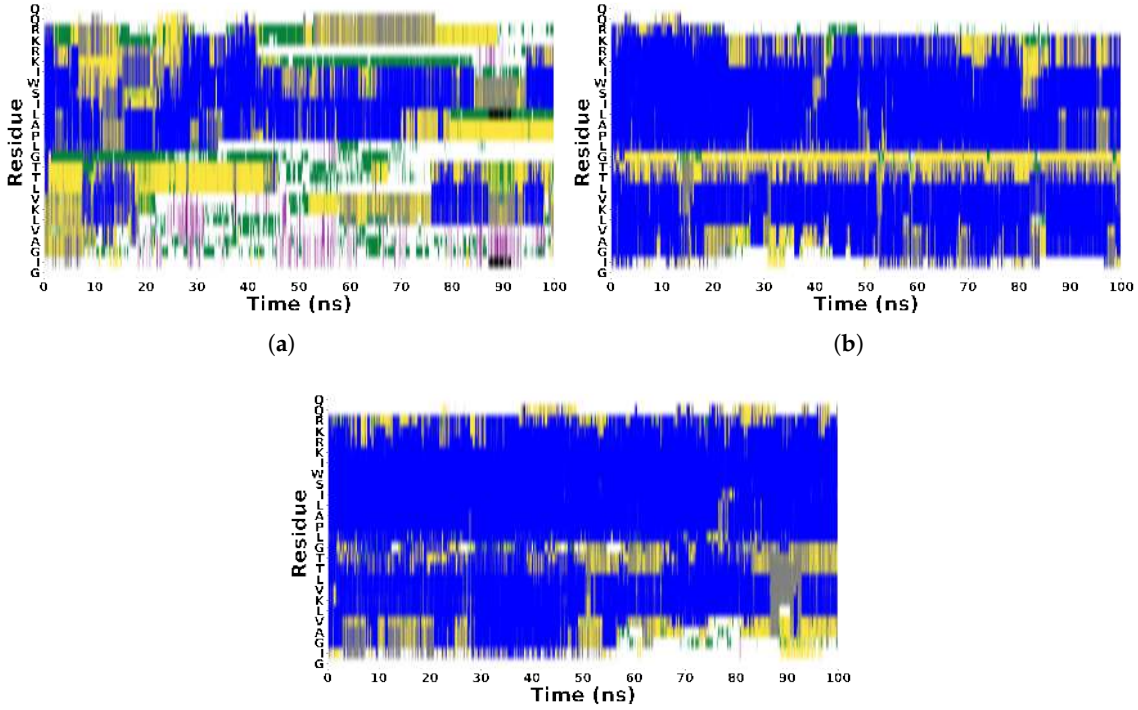

(**a**) (**b**)

(**c**)

Figure 6. Evolution of secondary structure from DSSP algorithm of MLT in water (**a**), 30% (*v*/*v*) TFE/water (**b**), and 30% (*v*/*v*) HFIP/water (**c**) solutions during 100 ns of MD simulations. Color Code: Coil α-Helix Bent Turn π-Helix 3-Helix.

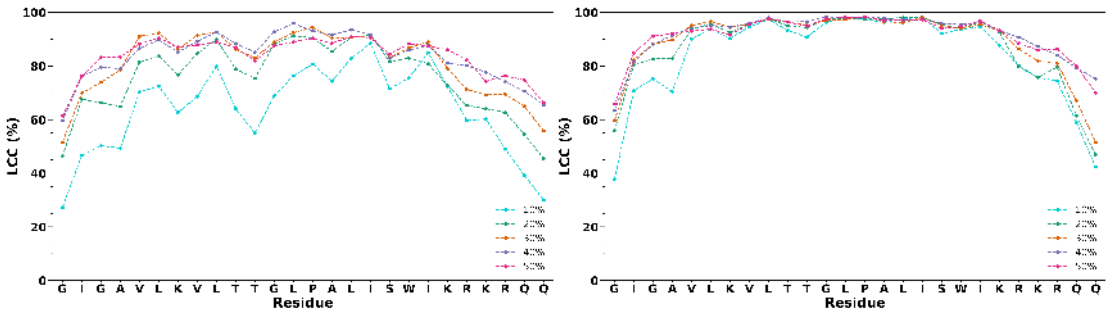

(**a**) (**b**)

Figure 7. Local cosolvent concentration for C_α atom of each residue of MLT in cosolvent/water solutions of TFE (**a**) and HFIP (**b**) at 6 Å.

https://doi.org/10.3390/liquids6010006

4. Conclusions

In this study, we have shown the results obtained by performing molecular dynamics simulations using an upgraded GAFF2 force field to simulate TFE and HFIP water solutions at several concentrations. The same force field has also been used to simulate Mellitin in several cosolvent/water mixtures to verify its efficacy in stabilizing the secondary structure. The thermodynamic properties of cosolvent/water solutions are in agreement with experimental findings, although the calculation of the static dielectric constant requires in-depth analysis. The new force field allows a correct description of the secondary structure of MLT in a range of concentrations from 10% to 50% v/v of cosolvent, showing that maximum helical stabilization is reached for a biosolvent concentration of 30% v/v, in full agreement with experimental evidence. The different analyses performed on molecular dynamics simulations afford an accurate characterization the structure of the peptide and the spatial organization of the cosolvent around the MLT, showing that TFE/HFIP molecules cluster near the central peptide backbone and side chains, displacing bulk water. In particular, for a biosolvent concentration in the range 30–40% v/v, we showed that the TFE/HFIP "coating" of MLT increases in the inner residues, leaving the C- and N-termini more exposed to water. Our results provide a thorough and convincing explanation of the stabilization effect of the helical structure in MLT promoted by the mixing of biosolvents in water.

Supplementary Materials: The following supporting information can be downloaded at: https://www.mdpi.com/article/doi/s1. Table S1: Calculated and experimental thermodynamic properties. Table S2: Average number of cosolvent and water molecules calculated at the first minimum of g(r). Figures S1 and S2: snapshot of the final frame from the MD simulation for three concentrations of TFE and HFIP water solutions. Figures S3–S10: evolution of secondary structure from DSSP algorithm of MLT in TFE/water and HFIP/water solutions. Figure S11: snapshots of the final frame from the MLT MD simulations for two cosolvent/water concentrations (10% and 50%). Video hfip_40.mpg: MLT in HFIP/water solutions at a concentration of 40% (v/v).

Author Contributions: Conceptualization, M.C. and M.M.; methodology, M.C., M.P., P.P. and M.M.; validation, M.C., M.P., C.A., A.M.P., P.P. and M.M.; formal analysis, M.C.; investigation, M.C. and M.M.; resources, C.A. and A.M.P.; data curation, M.C. and M.M.; writing—review and editing, M.C., M.P., C.A., A.M.P., P.P. and M.M.; visualization, M.C.; supervision, M.P., P.P. and M.M.; project administration, M.M. All authors have read and agreed to the published version of the manuscript.

Funding: This research received no external funding.

Data Availability Statement: The data to perform MD simulations will be made available by the authors on request. The data supporting the conclusions are contained within the article.

Acknowledgments: The authors thank MUR-Italy ("Progetto Dipartimenti di Eccellenza 2023-2027" allocated to Department of Chemistry "Ugo Schiff") and the National Recovery and Resilience Plan, Mission 4 Component 2-Investment 1.4-NATIONAL CENTER FOR HPC, BIG DATA AND QUANTUM COMPUTING—funded by the European Union-NextGenerationEU-CUP B83C22002830001. Calculations were performed in the LEONARDO HPC cluster, for which we acknowledge the CINECA award under the ISCRA initiative (HP10C06NZI) for the availability of high-performance computing resources and support.

Conflicts of Interest: The authors declare no conflicts of interest.

References

1. Searle, M.S.; Zerella, R.; Williams, D.H.; Packman, L.C. Native-like β-hairpin structure in an isolated fragment from ferredoxin: NMR and CD studies of solvent effects on the N-terminal 20 residues. *Protein Eng. Des. Sel.* **1996**, *9*, 559–565. [CrossRef]
2. Buck, M. Trifluoroethanol and colleagues: Cosolvents come of age. Recent studies with peptides and proteins. *Q. Rev. Biophys.* **1998**, *31*, 297–355. [CrossRef] [PubMed]
3. Hong, D.P.; Hoshino, M.; Kuboi, R.; Goto, Y. Clustering of fluorine-substituted alcohols as a factor responsible for their marked effects on proteins and peptides. *J. Am. Chem. Soc.* **1999**, *121*, 8427–8433. [CrossRef]
4. Roccatano, D.; Colombo, G.; Fioroni, M.; Mark, A.E. Mechanism by which 2,2,2-trifluoroethanol/water mixtures stabilize secondary-structure formation in peptides: A molecular dynamics study. *Proc. Natl. Acad. Sci. USA* **2002**, *99*, 12179–12184. [CrossRef]
5. Ramirez, L.S.; Pande, J.; Shekhtman, A. Helical Structure of Recombinant Melittin. *J. Phys. Chem. B* **2019**, *123*, 356–368.
6. Fioroni, M.; Burger, K.; Mark, A.E.; Roccatano, D. Model of 1,1,1,3,3,3-hexafluoro-propan-2-ol for molecular dynamics simulations. *J. Phys. Chem. B* **2001**, *105*, 10967–10975. [CrossRef]
7. Fioroni, M.; Burger, K.; Mark, A.E.; Roccatano, D. A New 2,2,2-trifluoroethanol Model for Molecular Dynamics Simulations. *J. Phys. Chem. B* **2000**, *104*, 12347–12354. [CrossRef]
8. Macchiagodena, M.; Mancini, G.; Pagliai, M.; Del Frate, G.; Barone, V. Fine-tuning of atomic point charges: Classical simulations of pyridine in different environments. *Chem. Phys. Lett.* **2017**, *677*, 120–126. [CrossRef]
9. Macchiagodena, M.; Mancini, G.; Pagliai, M.; Cardini, G.; Barone, V. New atomistic model of pyrrole with improved liquid state properties and structure. *Int. J. Quantum Chem.* **2018**, *118*, e25554. [CrossRef]
10. Macchiagodena, M.; Pagliai, M.; Andreini, C.; Rosato, A.; Procacci, P. Upgraded AMBER Force Field for Zinc-Binding Residues and Ligands for Predicting Structural Properties and Binding Affinities in Zinc-Proteins. *ACS Omega* **2020**, *5*, 15301–15310. [CrossRef]
11. Macchiagodena, M.; Pagliai, M.; Andreini, C.; Rosato, A.; Procacci, P. Upgrading and Validation of the AMBER Force Field for Histidine and Cysteine Zinc(II)-Binding Residues in Sites with Four Protein Ligands. *J. Chem. Inf. Model.* **2019**, *59*, 3803–3816. [CrossRef] [PubMed]
12. Casoria, M.; Macchiagodena, M.; Rovero, P.; Andreini, C.; Papini, A.M.; Cardini, G.; Pagliai, M. Upgrading of the general AMBER force field 2 for fluorinated alcohol biosolvents: A validation for water solutions and melittin solvation. *J. Pept. Sci.* **2024**, *30*, e3543. [CrossRef] [PubMed]
13. Wang, J.; Wolf, R.M.; Caldwell, J.W.; Kollman, P.A.; Case, D.A. Development and testing of a general amber force field. *J. Comput. Chem.* **2004**, *25*, 1157–1174. [CrossRef] [PubMed]
14. Kemple, M.D.; Buckley, P.; Yuan, P.; Prendergast, F.G. Main chain and side chain dynamics of peptides in liquid solution from 13C NMR: Melittin as a model peptide. *Biochemistry* **1997**, *36*, 1678–1688. [CrossRef]
15. Hirota, N.; Mizuno, K.; Goto, Y. Group additive contributions to the alcohol-induced α-helix formation of melittin: Implication for the mechanism of the alcohol effects on proteins. *J. Mol. Biol.* **1998**, *275*, 365–378. [CrossRef]
16. Abraham, M.J.; Murtola, T.; Schulz, R.; Páll, S.; Smith, J.C.; Hess, B.; Lindahl, E. GROMACS: High performance molecular simulations through multi-level parallelism from laptops to supercomputers. *SoftwareX* **2015**, *1-2*, 19–25. [CrossRef]
17. Lindorff-Larsen, K.; Piana, S.; Palmo, K.; Maragakis, P.; Klepeis, J.L.; Dror, R.O.; Shaw, D.E. Improved side-chain torsion potentials for the Amber ff99SB protein force field. *Proteins* **2010**, *78*, 1950–1958. [CrossRef]
18. Jorgensen, W.L.; Chandrasekhar, J.; Madura, J.D.; Impey, R.W.; Klein, M.L. Comparison of simple potential functions for simulating liquid water. *J. Chem. Phys.* **1983**, *79*, 926–935. [CrossRef]
19. Pagliai, M.; Macchiagodena, M.; Procacci, P.; Cardini, G. Evidence of a Low–High Density Turning Point in Liquid Water at Ordinary Temperature under Pressure: A Molecular Dynamics Study. *J. Phys. Chem. Lett.* **2019**, *10*, 6414–6418. [CrossRef]
20. Bussi, G.; Donadio, D.; Parrinello, M. Canonical sampling through velocity rescaling. *J. Chem. Phys.* **2007**, *126*, 014101. [CrossRef]
21. Hess, B.; Bekker, H.; Berendsen, H.J.; Fraaije, J.G. LINCS: A linear constraint solver for molecular simulations. *J. Comput. Chem.* **1997**, *18*, 1463–1472. [CrossRef]
22. Darden, T.; York, D.; Pedersen, L. Particle mesh Ewald: An N·log (N) method for Ewald sums in large systems. *J. Chem. Phys.* **1993**, *98*, 10089–10092. [CrossRef]
23. Allen, M.P.; Tildesley, D.J. *Computer Simulation of Liquids*; Oxford University Press: Oxford, UK, 1987.
24. Kabsch, W.; Sander, C. Dictionary of Protein Secondary Structure: Pattern Recognition of Hydrogen-bonded and Geometrical Features. *Biopolymers* **1983**, *22*, 2577–2637. [CrossRef] [PubMed]
25. Roccatano, D.; Fioroni, M.; Zacharias, M.; Colombo, G. Effect of hexafluoroisopropanol alcohol on the structure of melittin: A molecular dynamics simulation study. *Protein Sci.* **2005**, *14*, 2582–2589. [CrossRef] [PubMed]
26. Madelung, O. Static Dielectric Constants of Pure Liquids and Binary Liquid Mixtures. *Numer. Data Funct. Relationships Sci. Technol.* **1991**, *6*, 459. [CrossRef]
27. Rochester, C.; Symonds, J. Densities of solutions of four fluoroalcohols in water. *J. Fluor. Chem.* **1974**, *4*, 141–148. [CrossRef]

28. Cabani, S.; Gianni, P.; Mollica, V.; Lepori, L. Group contributions to the thermodynamic properties of non-ionic organic solutes in dilute aqueous solution. *J. Solut. Chem.* **1981**, *10*, 563–595. [CrossRef]
29. Marenich, A.V.; Kelly, C.P.; Thompson, J.D.; Hawkins, G.D.; Chambers, C.C.; Giesen, D.J.; Winget, P.; Cramer, C.J.; Truhlar, D.G. Minnesota Solvation Database (MNSOL) version 2012. Retrieved from the Data Repository for the University of Minnesota (DRUM), 2020. Available online: https://conservancy.umn.edu/items/c3db00cf-d573-461b-adf5-389ff929d918 (accessed on 9 October 2025).
30. Denda, M.; Touhara, H.; Nakanishi, K. Excess molar enthalpies for (water + a fluoroalkanol). *J. Chem. Thermodyn.* **1987**, *19*, 539–542. [CrossRef]
31. Caleman, C.; van Maaren, P.J.; Hong, M.; Hub, J.S.; Costa, L.T.; van der Spoel, D. Force Field Benchmark of Organic Liquids: Density, Enthalpy of Vaporization, Heat Capacities, Surface Tension, Isothermal Compressibility, Volumetric Expansion Coefficient, and Dielectric Constant. *J. Chem. Theory Comput.* **2012**, *8*, 61–74. [CrossRef]
32. Macchiagodena, M.; Mancini, G.; Pagliai, M.; Barone, V. Accurate prediction of bulk properties in hydrogen bonded liquids: Amides as case studies. *Phys. Chem. Chem. Phys.* **2016**, *18*, 25342–25354. [CrossRef]
33. García-Melgarejo, V.; Núñez-Rojas, E.; Alejandre, J. United atom model via interactions with explicit water (UAMI-EW): Alcohols and ketones. *J. Mol. Liq.* **2021**, *323*, 114576. [CrossRef]
34. Salas, F.J.; Núñez-Rojas, E.; Alejandre, J. Parameterization of phenol, benzoic acid and phenolic acids to obtain their solubility in water. *J. Mol. Liq.* **2025**, *427*, 127467. [CrossRef]
35. Gente, G.; La Mesa, C. Water—Trifluoroethanol Mixtures: Some Physicochemical Properties. *J. Solut. Chem.* **2000**, *29*, 1159–1172. [CrossRef]
36. Mainar, A.M.; Martínez-López, J.F.; Urieta, J.S.; Pardo, J.I. Solubility of gases in fluoroorganic alcohols. Part III. Solubilities of several non-polar gases in water+ 1, 1, 1, 3, 3, 3-hexafluoropropan-2-ol at 298.15 K and 101.33 kPa. *J. Chem. Thermodyn.* **2019**, *132*, 229–239. [CrossRef]
37. Harris, K.R.; Newitt, P.J.; Derlacki, Z.J. Alcohol tracer diffusion, density, NMR and FTIR studies of aqueous ethanol and 2,2,2-trifluoroethanol solutions at 25 °C. *J. Chem. Soc. Faraday Trans.* **1998**, *94*, 1963–1970. [CrossRef]